Available online at www.sciencedirect.com
ScienceDirect
Comput. Methods Appl. Mech. Engrg. 410 (2023) 116019
Computer methods in applied mechanics and engineering
www.elsevier.com/locate/cma

Single-track thermal analysis of laser powder bed fusion process: Parametric solution through physics-informed neural networks

E. Hosseini[a,*], P. Gh Ghanbari[a,b], O. Müller[a,b], R. Molinaro[c], S. Mishra[d]

[a] *Empa Swiss Federal Laboratories for Materials Science & Technology, Dübendorf, Switzerland*
[b] *Institute for Mechanical Systems, Department of Mechanical and Process Engineering, ETH Zürich, Switzerland*
[c] *Seminar for Applied Mathematics, Department of Mathematics, ETH Zürich, Switzerland*
[d] *Seminar for Applied Mathematics, Department of Mathematics and ETH AI Center, ETH Zürich, Switzerland*

Received 12 February 2023; received in revised form 15 March 2023; accepted 16 March 2023
Available online xxxx

Abstract

Modelling the highly localised and rapid phenomena occurring during metal additive manufacturing (MAM) processes such as the laser powder bed fusion (LPBF) demands the adoption of very fine time- and space-discretisation and therefore high computational cost for the classical simulation approaches, namely the finite element method (FEM). Particularly, when the solution is required for a range of scenarios, e.g. in sensitivity or optimisation analyses, computation costs of such simulations are not affordable. As an alternative strategy, this study explores the application of physics informed neural networks (PINNs) as a low-cost physics-based simulation approach for the thermal analysis of the LPBF process, through which reliable transient and steady-state temperature profiles for single-track LPBF depositions are achieved. An unsupervised learning strategy is employed for PINNs to parametrically solve the heat transfer equation for the LPBF process. The trained PINNs calculate the temperature profiles and the melt-pool dimensions evolving during the LPBF process for any given set of material's thermal properties and process conditions at practically zero computational cost. The reliability of the PINNs outcomes is verified through ground-truth data generated based on several benchmark equivalent finite element simulations.

Keywords: Physics informed neural networks; Additive manufacturing; Thermal simulation; Parametric analysis

1. Introduction

Marking its evolution as a central feature of the fourth industrial revolution, additive manufacturing broadly refers to the layer-by-layer 'printing' of spatially precise on-demand 3D objects with enhanced design freedom relative to conventional technologies. Effective contribution of metal additive manufacturing (MAM) to the vision of Industry 4.0 necessitates addressing its key challenges in the cost and reliability of the printed parts [1]. The cost barrier to extensive adoption of MAM technology inherently arises from both the high costs of the production process (e.g. due to slow manufacturing and expensive feed materials) and the high rate of manufacturing failures [2,3]. The high production cost tends to move the application of the technology to specific cases where MAM can result

* Corresponding author.
E-mail address: ehsan.hosseini@empa.ch (E. Hosseini).

https://doi.org/10.1016/j.cma.2023.116019

in adequate value creation, i.e. fabrication of complex geometries, or where conventional manufacturing would be even more expensive, e.g. small batch production [4]. The more critical cost contributor for MAM originates from the difficulties in finding the *right* printing process parameters where non-optimal conditions can result in inferior quality or total failure of the printing process [5]. The problem can be due to local overheating, excessive distortion, cracking, high porosity, undesired microstructure, or poor mechanical properties, to name a few [6,7]. Currently, in the lack of a more intelligent solution, the time-consuming and expensive trial-and-error strategy based on numerous experiments is commonly adopted to optimise the process parameters for a given printing machine, material and part [3,8,9]. As an alternative, physics-based simulations can provide a deeper understanding of the complex phenomena occurring during MAM and hence guide for optimising the process conditions. When the computations are sufficiently fast, they can even be used to systematically control the process and contribute to achieving the goal of 'first-time-right' high-quality production.

Conventional methods for physics-based simulation of MAM suffer from high computational costs [10]. The underlying reason lies not only in the complexity of the phenomena occurring during MAM but also in their extraordinarily rapid and localised nature [11]. As a result, classical numerical analyses such as the finite element method (FEM) require very fine discretisations to solve system's governing partial differential equations (PDEs). To put this into perspective, the temperature gradients and cooling rates in the vicinity of the process zone in the LPBF process can be in the orders of 10^6 K/m and 10^6 K/s, respectively [12,13], which demands the adoption of micrometre-sized and microsecond-long space- and time-discretisation within the FEM framework. As an alternative to the classical numerical methods, this study explores applying physics informed neural networks (PINNs) for developing reliable and rapid analysis strategies for MAM. In contrast to black-box machine learning, PINNs do not simply learn from labelled data but (in an unsupervised fashion) seek a solution which satisfies the governing physical laws of systems, and therefore, are attractive from a scientific point of view. Importantly and superior to the conventional simulation methods, PINNs can perceive the sensitivity of the solution to input parameters and even provide a parametric solution to the problem, which is very beneficial for sensitivity analyses and applications where the solution is required for various scenarios [14,15].

To this end and as a preliminary investigation, this study focuses on adopting PINNs for (parametrically) solving the heat equation and calculating the induced temperature profiles during single-track LPBF depositions. After training, evaluating PINNs for predicting temperature profiles incurs a computational cost in the micro to millisecond range, which is several orders of magnitude shorter than that for the corresponding FE calculations. Initially, we assume a temperature-independent thermal behaviour for the material and develop PINNs to determine the temperature profiles for a range of thermal conductivities, specific heat capacities and densities during LPBF with various values for the laser power and scanning speed. The second PINNs account for the temperature dependence of thermal properties for Hastelloy X and calculate the temperature profiles and the melt-pool dimensions during the LPBF process for any given combination of laser powers and scanning speeds. This demonstrates the capability of PINNs to solve thermal problems while accounting for temperature-dependent material properties. Both PINNs are verified based on outcomes of several equivalent finite element simulations in a benchmark study.

2. Physics informed neural networks (PINNs)

Partial differential equations (PDEs) govern the response of many natural and man-made phenomena in science and technology. As analytical solutions are only available for a few types of PDEs, numerical simulation methods such as finite difference, finite element, and finite volume are often employed for practical problems. Although successful in many cases, the computational cost of such numerical approaches for application to complex systems is prohibitively high, particularly for problems in which the solution to the PDEs is required for various scenarios [14,15], e.g. for sensitivity analysis, uncertainty quantification and optimisation problems.

In the past few years, machine learning has emerged as a central tool in scientific computing, and deep learning is considered an effective method for the numerical approximation of PDEs [16]. Importantly, deep neural networks (DNNs) possess the so-called universal approximation property or the ability to approximate any continuous function and, therefore, can be the ansatz spaces for the solutions of PDEs [17]. This is the underlying idea of PINNs, first proposed by Lagaris et al. [18,19] and revived and further developed after 2019 by Karniadakis and collaborators [20,21]. In contrast to the conventional machine learning tools in data science which require large amounts of labelled data-sets, training of PINNs does not necessarily need any labelled data-sets and PINNs can be purely thought of as unsupervised learners for solving PDEs [22].

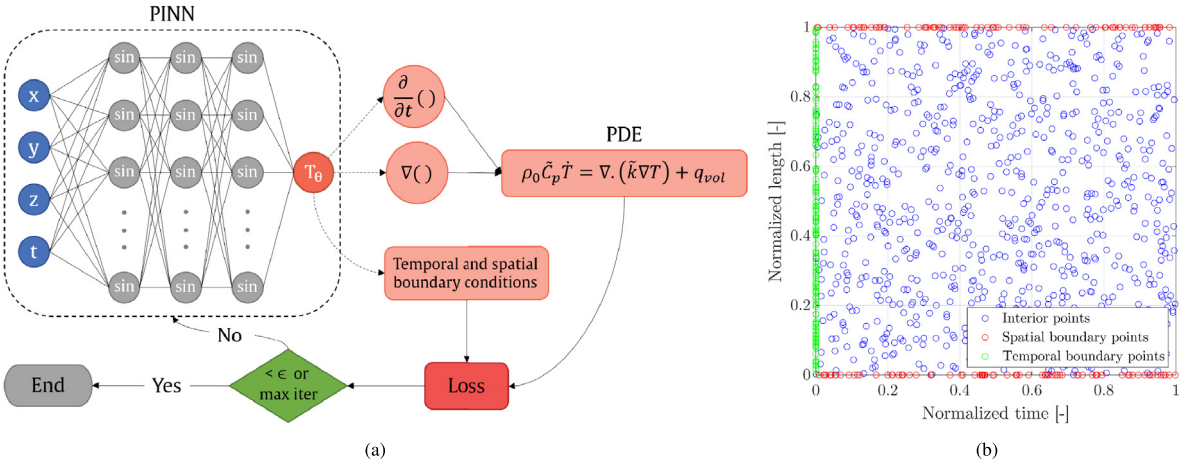

Fig. 1. (a) A schematic diagram of the physics informed neural network for solving the heat equations where the loss function contains a mismatch in the temporal and spacial boundary conditions and the residuals for the PDE on a set of collocation points in the time–space(-parameters) domain. (b) low-discrepancy Sobol sampling for interior, spatial and temporal boundary collocation points.

Assuming the example of thermal simulation of LPBF process, it is desired to solve the governing PDE of $D(T) = f$ (heat equation) and determine T (temperature field) as a function of $\boldsymbol{y}$ (space, time, and material/process parameters) such that it satisfies the given temporal and spacial boundary conditions. The following describes the application of PINNs for solving such a problem.

A feed-forward DNN might be considered to transform input $\boldsymbol{y}$ to output T through layers of neurons, which are composed of affine-linear maps between neurons in successive layers and a scalar nonlinear activation function [23]. Mathematically and for the shown K-layer DNN in Fig. 1(a) [15]:

$$T_\theta(\boldsymbol{y}) = C_K \circ \sigma \circ C_{K-1} \circ \ldots \sigma \circ C_2 \circ \sigma \circ C_i(\boldsymbol{y}) \tag{1}$$

where $\circ$ refers to the composition of functions. The network has $K-1$ hidden layers where kth hidden layer transforms an input vector z_k by an affine linear function C_k, i.e. $C_k(z_k) = W_k z_k + b_k$, and then by a scalar (nonlinear) activation function σ (*logistic*, *sin*, *tanh*, etc. [23]). Training of DNNs is searching for the best concatenated set of tuning parameters $\theta = \{W_k, b_k\}$ using gradient descent methods such that the mismatch between the neural network and the underlying target is minimised [15]. Assuming T_θ is the approximate solution of the PDE of $D(T) = f$, therefore, the tuning parameters should be found to minimise the following residual [15,18].

$$R_{PDE} = D(T_\theta) - f \tag{2}$$

Additionally, the solution should satisfy the temporal and spacial boundary conditions of the problem (i.e. minimise R_{BC}), and therefore, it can be stated that training of PINNs involves a search to find a set of θ^* such [15]:

$$\theta^* = argmin\,(R_{PDE} + \lambda R_{BC}) \tag{3}$$

The solution to the above minimisation problem does not necessitate access to 'labelled training data' and can be seen as unsupervised learning. PINN is a grid-less approach and the strategy proposed by LeCun et al. [24] suggests evaluating and minimising the residuals for a chosen set of 'collocation' points $\{\boldsymbol{y}_n\}$, see Fig. 1(b). Commonly, the low-discrepancy *Sobol* sampling strategy is adopted for creating the collocation point set [25], while it is found in this study that a more clever sampling strategy, inspired by the physics of the problem, might be required for 'spiky' problems, i.e. situations where the gradients of the field variables in certain small regions are particularly large.

Coding and implementation of PINNs, e.g. within the *PyTorch* framework, is extremely simple and only needs a few lines of Python code. In contrast to the classical simulation approaches based on numerical schemes for differentiation, PINNs employ differential operators on graphs and use GPU-accelerated automatic differentiation

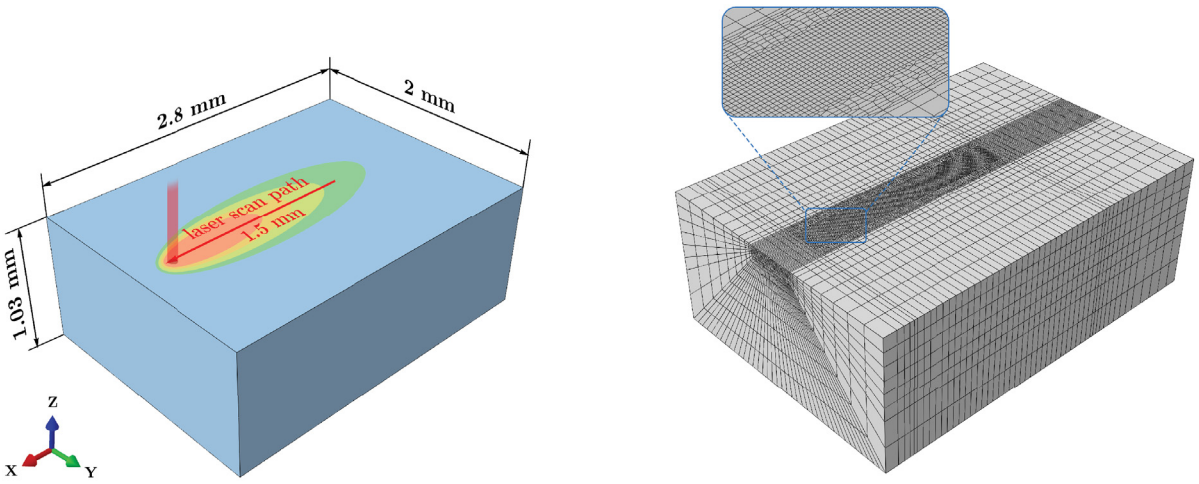

Fig. 2. (a) Details for the evaluated thermal problem, (b) the designed FE mesh in ABAQUS [5] to generate *'ground-truth'* data for evaluating accuracy of PINNs solutions.

to elegantly and efficiently calculate the derivative operators of the governing equations and those required in the gradient descent method for the training of the neural networks. [26,27]. Importantly, PINNs are very well suited for solving parametric PDEs [28], i.e. for situations where the solution to the governing PDE is required for different scenarios (e.g. different material parameters and process conditions for thermal analysis of the LPBF process). A solution to such a problem through classical numerical solvers needs individual simulations for each scenario and is prohibitively costly.

3. PINNs for thermal analysis of LPBF process

The main objective of this study is to calculate the transient and steady-state temperature profiles (and melt pool dimensions) during single-track LPBF depositions for any given process parameters and material's thermal properties. It is well known that the induced temperature profiles by the laser stabilise after <1.5 mm from the start of a track in the LPBF process [29]. Therefore, to include both transient and steady thermal states, analyses are conducted for a 1.5 mm long laser track within a large-enough domain with the dimensions of $2.8\times2.0\times1.0\,\text{mm}^3$ (L×W×H), Fig. 2(a).

Following [30–33], this study employed the continuum modelling strategy for the thermal analysis of the LPBF process. This method takes simplifications such as ignoring explicit modelling of individual powder particles or phenomena related to molten metal motion in the analysis. The relevance of such a strategy for predicting temperature profiles during LPBF has been evaluated and discussed in [30,33]. More detailed simulations considering two-phase thermo-fluid dynamics are essential, if the prediction of additional features such as the risk of defect formation during the deposition process is aimed. Such a strategy has not been followed in this study, and the focus is on using the continuum framework and exploring PINNs for providing a reliable and rapid parametric solution for the heat equation, applied to the thermal analysis of LPBF single-track depositions.

Accordingly, a time-dependent temperature field $T\,(x, y, z, t, \ldots)$ is sought to satisfy the below thermal energy conservation equation (and the given temporal and spacial boundary conditions):

$$\rho_0 \tilde{C}_p \dot{T} = \nabla.\left(\tilde{k}\nabla T\right) + q_{vol} \tag{4}$$

Here ρ_0, $\tilde{C}_p$ and $\tilde{k}$ are the reference density, apparent specific heat capacity, and effective thermal conductivity, respectively, and q_{vol} is the volumetric heat generation term representing the contribution of laser energy source. The apparent specific heat capacity is a temperature-dependent quantity that deviates from the material's specific heat capacity C_p in the temperature ranges relevant to a phase transformation, accounting for the associated enthalpy

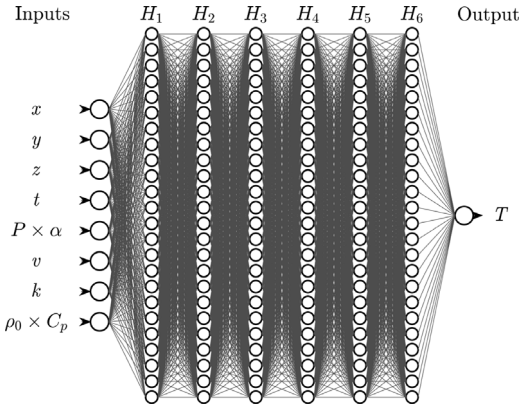

Fig. 3. Schematics of the developed PINNs for the thermal analysis of the LPBF process.
Source: Image created with [40].

changes [34]. The effective thermal conductivity is also a temperature-dependent quantity that deviates from the material's thermal conductivity k at temperatures higher than the melting point to account for the heat distribution induced by convection of molten metal due to Marangoni and buoyancy mechanisms [32,35]. Since this thermal analysis does not solve for the displacement field, the density at the reference configuration needs to be considered to maintain a consistent mass for the system [32,36], i.e. $\rho_0 = 8352\,\mathrm{kg\,m^{-3}}$ for Hastelloy X at 25 °C.

The volumetric heat generation term q_{vol} in Eq. (4) can be considered as a semi-spherical heat source centred at the location of the laser [35,37]:

$$q_{vol} = \alpha \frac{6\sqrt{3}P}{\pi\sqrt{\pi}r^3} \exp\left(-3\frac{(x+vt)^2+y^2}{r^2}\right) \exp\left(-3\frac{z^2}{c^2}\right) \tag{5}$$

where P is the laser power, α is the laser absorption coefficient, r is the laser radius, c is the laser penetration depth, and v is the laser scan speed (discussions on more advanced formulations for considering the laser heat source can be found in [38]).

An initial temperature of 25 °C is considered for the model, and heat losses due to convection and radiation from the top surface are neglected, after Pinkerton and Lin [39] who reported negligible influence from such consideration. It should however be noted that other initial/boundary conditions can be equivalently implemented into PINNs.

Solving the above problem for a few given sets of process and material parameters through FEM is straightforward and is used in this study to establish the *'ground-truth'* results for evaluating the accuracy of PINNs solutions (i.e. not for training PINNs). Fig. 2(b) shows the generated FE mesh, which employs small elements only in the vicinity of the laser path to increase the efficiency of the computations [5]. The model has 110k nodes and 102k elements with the characteristics size of 10 μm close to the laser path and up to 150 μm elements on the outer boundaries of the domain. The FE solution of the above problem using 12 threads of an Intel Xeon Gold 6150 CPU took ∼2.5 h and ∼0.2 h with and without consideration of temperature dependence of the material's thermal properties, respectively. Considering temperature-dependent thermal properties introduces nonlinearities that necessitate the adoption of smaller time increments and more iterations for the solver to converge, which leads to a higher computational cost. It is evident that FEM can be used neither for generating real-time simulation data nor in sensitivity analyses where the solution for a large span of process and material parameters is required.

In this study, we aim to use PINNs and construct a generalised (parametric) solution for Eq. (4) which gives the temperatures not only as a function of time and space but also as a function of process and material parameters, namely laser power, absorption coefficient, laser scan speed, density, conductivity, and heat capacity. It can be deduced from Eqs. (4) & (5) that the effect of laser power and absorption coefficient, as well as that for heat capacity and density, are coupled and therefore can be combined for the generalised solution of Eq. (4).

Fig. 3 illustrates a schematic of the developed PINNs for the thermal analysis of the LPBF single-track depositions. A fully connected feed-forward neural network with six hidden layers of 24 neurons each with *sin*

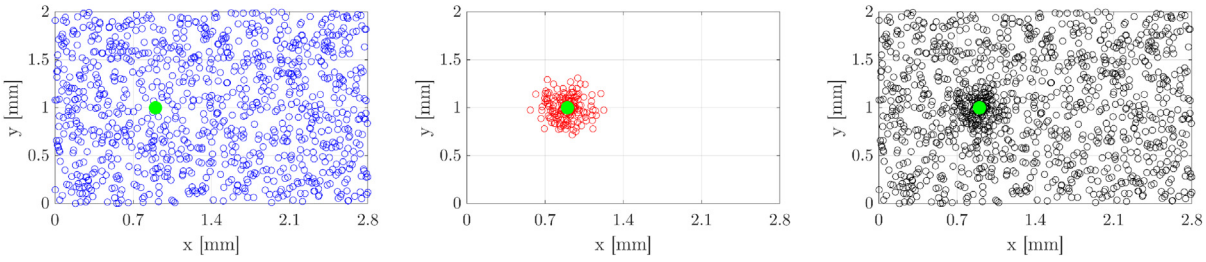

Fig. 4. (a) 2D schematics of low-discrepancy Cartesian Sobol sampling, (b) random Spherical collocation point sampling, centred at the location of the moving heat source, (c) superposition of samplings shown in (a) and (b) to form the adopted interior collocation points for PINNS. Note that the green circle presents the temporal location of the laser heat source. (For interpretation of the references to colour in this figure legend, the reader is referred to the web version of this article.)

activation functions is constructed. This architecture has been chosen based on the results of an ensemble training exercise (the Github repository contains all the relevant information about the network and its training parameters).

The network takes eight inputs: three spatial coordinates, time, laser power × absorption coefficient, laser scanning speed, thermal conductivity, and specific heat capacity × reference density, and gives the temperature as the output. Training the network involves optimising the weights and biases (ca. 3K unknown values) based on the LBFGS algorithm [41] for 2^{19} collocation points. The number of collocation points is selected such that the memory capacity of the employed GPU allows a batch size of one for the training.

Importantly, it is found that efficient network training is only feasible through consideration of a nonhomogeneous distribution of the interior collocation points such that a higher population exists in the vicinity of the moving laser heat source, where higher temperature gradients are expected (resampling a 'spiky' problem). For such a purpose, a random spherical collocation point distribution [42], centred at the location of the moving heat source and with a radius of 300 µm, is adopted for 10% of the interior collocation points (Fig. 4(b)). This distribution is superimposed on a Cartesian Sobol collocation point distribution (Fig. 4(a)) to construct the interior collocation point set used for the calculation of R_{PDE}, as presented in Fig. 4(c). This idea resembles the cumbersome adaptive re-meshing strategy in FEM, i.e. continues change of the mesh during calculation. Implementation of this concept into PINNs is very straightforward and does not affect the computational cost, i.e. in total contrast to its counterpart for the FEM.

The network is trained for two scenarios. PINNs-I are trained without consideration of the temperature dependence of the material's thermal properties to estimate temperature as $T = T\left(x, y, z, t, P \times \alpha, v, k, \rho_0 \times C_p\right)$. In the next step and to demonstrate the capability of PINNs to deal with nonlinearities induced from considering temperature-dependent material properties, thermal properties of LPBF Hastelloy X (Fig. 5) are employed to train PINNs-II and calculate the temperature profile as $T = T\left(x, y, z, t, P \times \alpha, v\right)$. With consideration of the melting temperature of 1345 °C for Hastelly X, the outcomes of PINNs-II are also assessed to calculate the dimensions of the LPBF melt pool i.e. $D_{meltpool} = D_{meltpool}\left(P \times \alpha, v\right)$.

Training of PINNs is performed on a single Nvidia Titan RTX GPU and took ∼1.8 h and ∼4 h for PINNs-I and PINNs-II, respectively. After the training, the evaluation of networks for calculating temperature profiles for any combination of process and material parameters is at practically zero computational cost (1 ms for 1K network evaluations) which makes them ideal for real-time simulations and ultimately control and optimisation of the LPBF process. Another advantage of PINNs over FEM is the small disk-size of the final solution, which is a couple of megabytes for the whole range of process-material parameters for the former, but can be upwards of a gigabyte for every single scenario for the latter method.

4. Accuracy evaluation

The verification of the PINNs solutions in this study is based on comparing their outcomes with those from several benchmark equivalent FEM simulations. A random hypercube sampling strategy [44] is used to design six benchmarking cases to evaluate the accuracy of each PINNs solution. Tables 1 and 2 describe the training ranges

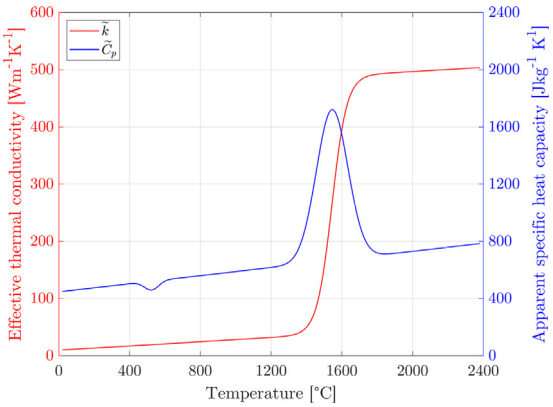

Fig. 5. Thermal properties of LPBF Hastelloy X [43].

Table 1
Training and benchmark evaluation conditions for PINNs-I.

Parameter Unit	K [W m^{-1} K^{-1}]	$\rho_0 \times C_p$ [mJ m^{-3} K^{-1}]	$P \times \alpha$ [W]	v [m s^{-1}]
Training range	5–20	2–5	10–20	0.5–1.5
Benchmark # 1	13.30	2.65	18.84	0.87
Benchmark # 2	8.14	3.86	15.08	0.80
Benchmark # 3	10.86	2.45	12.60	1.09
Benchmark # 4	7.07	4.59	17.70	1.23
Benchmark # 5	19.02	4.48	11.61	0.59
Benchmark # 6	15.61	3.48	14.47	1.37

Table 2
Training and benchmark evaluation conditions for PINNs-II.

Parameter Unit	$P \times \alpha$ [W]	v [m s^{-1}]
Training range	50–100	0.5–1.5
Benchmark # 1	94.45	1.00
Benchmark # 2	71.52	0.55
Benchmark # 3	60.83	0.98
Benchmark # 4	87.18	1.47
Benchmark # 5	80.82	0.80
Benchmark # 6	50.14	1.22

of the two PINNs as well as the conditions for their benchmark evaluation. The percentage Mean Absolute Error (MAE) is employed as an index in the assessment of the accuracy of PINNs solutions, i.e.:

$$\bar{\delta} = \left(\frac{\left| \bar{T}_{PINNs} - \bar{T}_{FEM} \right|}{\left| \bar{T}_{FEM} \right|} \right) \times 100 \tag{6}$$

where $\bar{T}_{PINNs}$ and $\bar{T}_{FEM}$ are the average of PINNs and FEM calculated temperatures. Fig. 6 compares the PINNs-I and FE calculated transient and steady-state temperature data for the conducted benchmark evaluations. As can be seen, PINNs can provide a close approximation of the FEM results, where the MAE remains below 4.5%.

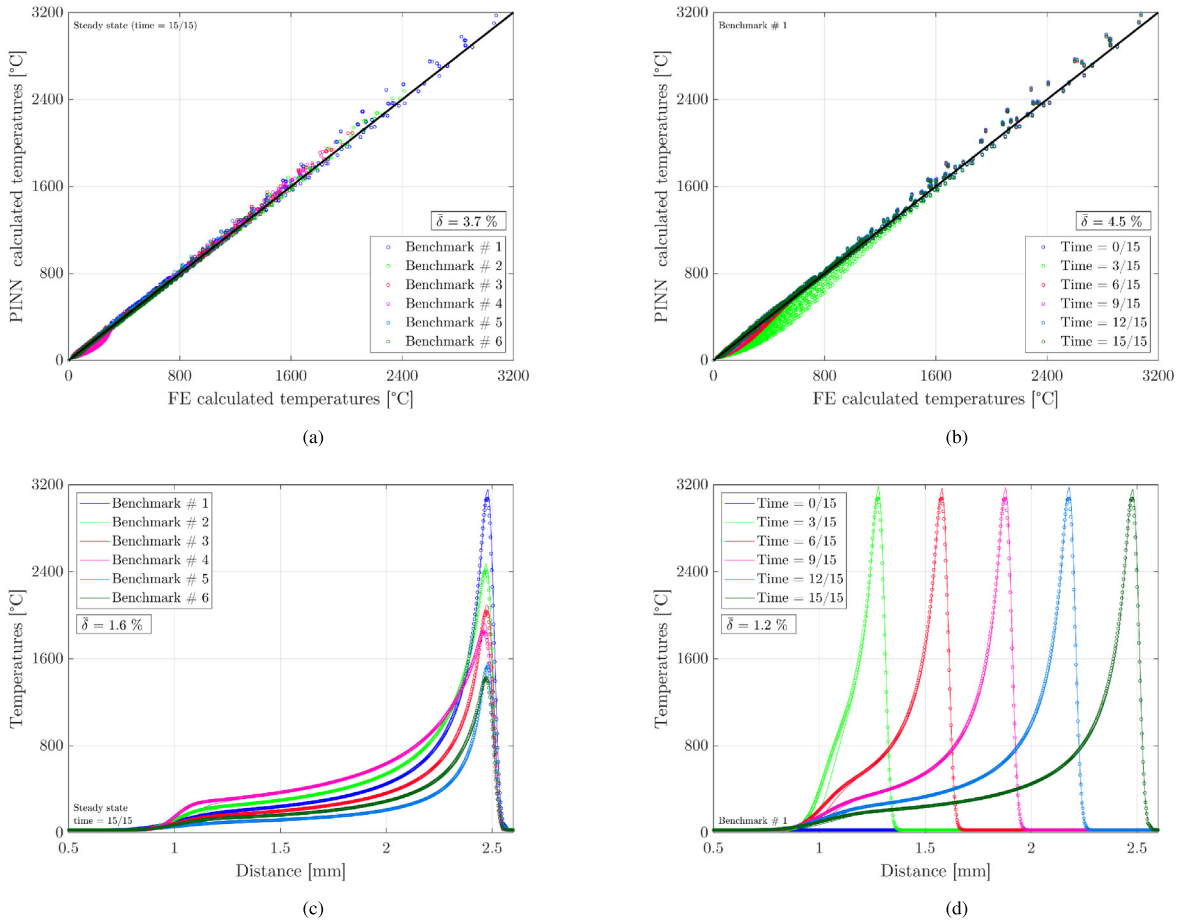

Fig. 6. Comparison of calculated temperatures from PINNs-I and corresponding FEM simulations in benchmark cases. (a) steady-state temperature distributions in six cases, (b) transient and steady-state temperatures for the first benchmark, (c) temperature profiles along the laser path for the last frame of analysis for the six cases, (d) evolution of temperature profile along the laser path in the first case.

Fig. 7 illustrates the PINNs-II calculated transient and steady-state temperature data and melt pool dimensions versus those derived from the equivalent FEM simulations. It can be observed from Figs. 6(c) & 6(d) and Figs. 7(c) & 7(d) that consideration of the temperature-dependent material properties significantly influences the shape of the temperature profiles. Similar to that for PINNs-I, the observations from Fig. 7 indicate that PINNs-II can acceptably represent the outcomes of FEM simulations for the conducted benchmark evaluations.

5. Concluding remarks

Reliable simulation tools are required for optimising and ultimately controlling metal additive manufacturing (MAM) systems to improve the process efficiency and quality of the builds. However, the high computational cost of classical simulation approaches such as the finite element method for analysing the MAM process does not allow their exploitation to this end. This study develops a reliable and rapid alternative for (single-track) thermal analysis of the laser powder bed fusion (LPBF) process based on physics informed neural networks (PINNs). The outstanding advantage of the developed PINNs solutions is that, after unsupervised training, they calculate the transient and steady temperature profiles (and consequently the melt-pool dimensions) during the LPBF process for any combination of the material's thermal properties and process conditions at practically zero computational cost. A benchmark study compares the outcomes of the developed PINNs with those from a series of equivalent FEM simulations and indicates Mean Absolute Error of below 5% for PINNs solutions.

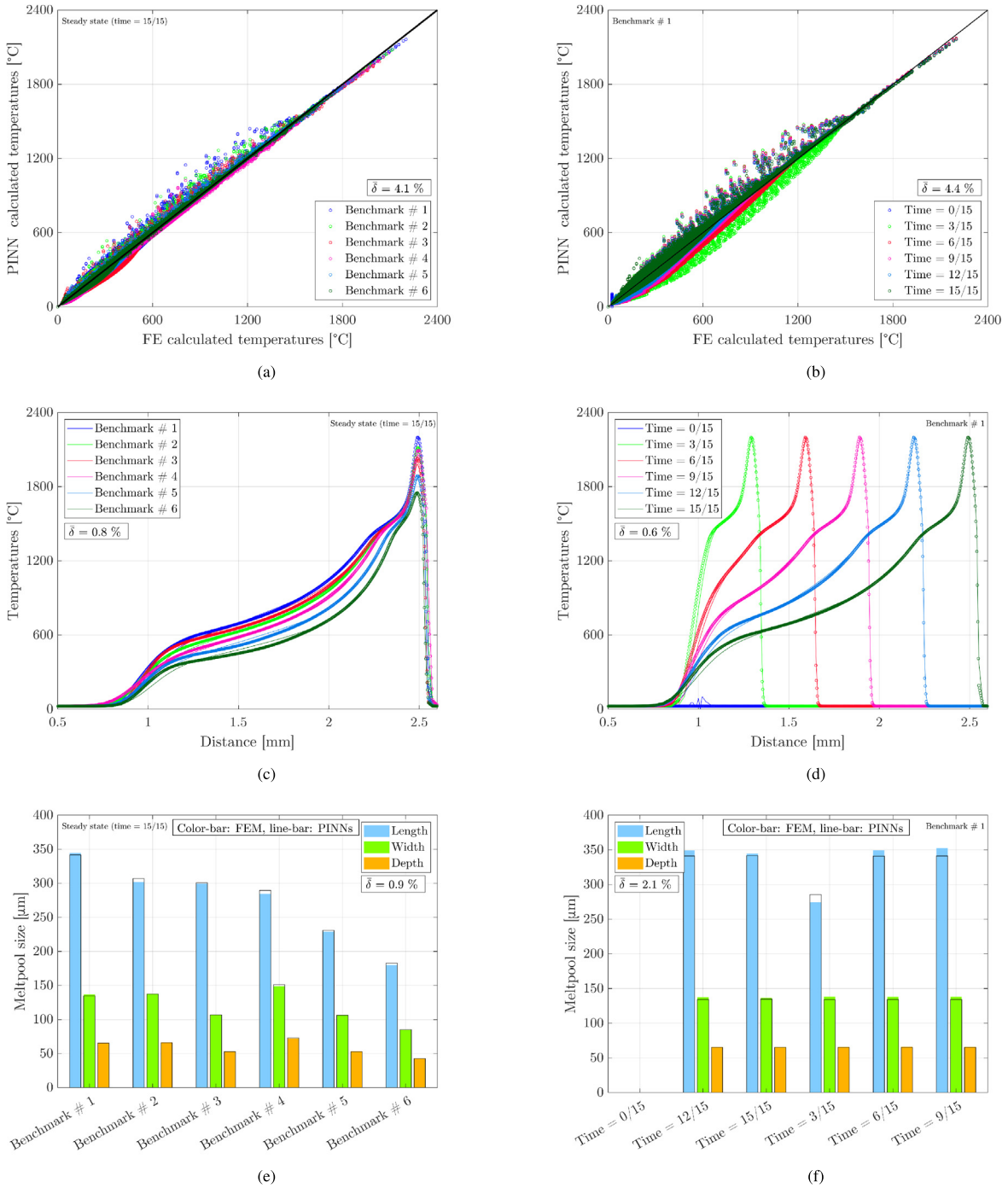

Fig. 7. Comparison of calculated temperatures and melt pool dimensions from PINNs-II and corresponding FEM simulations in benchmark cases. (a) steady state temperature distributions in six cases, (b) transient and steady-state temperatures for the first benchmark, (c) temperature profiles along the laser path for the last frame of analysis for the six cases, (d) evolution of temperature profile along the laser path in the first case, (e) steady-state melt pool dimensions for the six cases, (f) evolution of melt pool size in the first benchmark case.

Declaration of competing interest

The authors declare that they have no known competing financial interests or personal relationships that could have appeared to influence the work reported in this paper.

Data availability

Data will be made available on request

Acknowledgements

Financial support by the Swiss National Science Foundation, Switzerland (SNSF; grant number 200551) is gratefully acknowledged.

Appendix A. Supplementary materials

The models and scripts used in this study can be downloaded from https://github.com/HighTempIntegrity/LPBF_PINNs_2023

References

[1] Mahesh Mani, Shaw Feng, Brandon Lane, Alkan Donmez, Shawn Moylan, Ronnie Fesperman, Measurement Science Needs for Real-Time Control of Additive Manufacturing Powder Bed Fusion Processes, US Department of Commerce, National Institute of Standards and Technology, 2015.
[2] Jonas Barsing, A cost breakdown and production uncertainty analysis of additive manufacturing: a study of low-volume components produced with selective laser melting, 2018.
[3] T. DebRoy, T. Mukherjee, J.O. Milewski, J.W. Elmer, B. Ribic, J.J. Blecher, W. Zhang, Scientific, technological and economic issues in metal printing and their solutions, Nature Mater. 18 (10) (2019) 1026–1032.
[4] Simon Ford, Mélanie Despeisse, Additive manufacturing and sustainability: an exploratory study of the advantages and challenges, J. Clean. Prod. 137 (2016) 1573–1587.
[5] William J. Sames, F.A. List, Sreekanth Pannala, Ryan R. Dehoff, Sudarsanam Suresh Babu, The metallurgy and processing science of metal additive manufacturing, Int. Mater. Rev. 61 (5) (2016) 315–360.
[6] Dong Dong Gu, Wilhelm Meiners, Konrad Wissenbach, Reinhart Poprawe, Laser additive manufacturing of metallic components: materials, processes and mechanisms, Int. Mater. Rev. 57 (3) (2012) 133–164.
[7] E. Hosseini, V.A. Popovich, A review of mechanical properties of additively manufactured Inconel 718, Addit. Manuf. 30 (2019) 100877.
[8] Tridibesh Mukherjee, Tarasankar DebRoy, A digital twin for rapid qualification of 3D printed metallic components, Appl. Mater. Today 14 (2019) 59–65.
[9] Ian Gibson, David W. Rosen, Brent Stucker, Mahyar Khorasani, David Rosen, Brent Stucker, Mahyar Khorasani, Additive Manufacturing Technologies, Vol. 17, Springer, 2021.
[10] Lihang Yang, Tuğrul Özel, Physics-based simulation models for digital twin development in laser powder bed fusion, Int. J. Mechatronics Manuf. Syst. 14 (2) (2021) 143–163.
[11] P. Gh Ghanbari, Edoardo Mazza, Ehsan Hosseini, Adaptive local-global multiscale approach for thermal simulation of the selective laser melting process, Addit. Manuf. 36 (2020) 101518.
[12] H.K. Rafi, N.V. Karthik, Haijun Gong, Thomas L. Starr, Brent E. Stucker, Microstructures and mechanical properties of Ti6Al4V parts fabricated by selective laser melting and electron beam melting, J. Mater. Eng. Perform. 22 (12) (2013) 3872–3883.
[13] Neil J. Harrison, Iain Todd, Kamran Mumtaz, Reduction of micro-cracking in nickel superalloys processed by Selective Laser Melting: A fundamental alloy design approach, Acta Mater. 94 (2015) 59–68.
[14] Siddhartha Mishra, Roberto Molinaro, Estimates on the generalization error of physics-informed neural networks for approximating a class of inverse problems for PDEs, IMA J. Numer. Anal. 42 (2) (2022) 981–1022.
[15] Siddhartha Mishra, Roberto Molinaro, Estimates on the generalization error of physics-informed neural networks for approximating PDEs, IMA J. Numer. Anal. (2022).
[16] Salvatore Cuomo, Vincenzo Schiano Di Cola, Fabio Giampaolo, Gianluigi Rozza, Maizar Raissi, Francesco Piccialli, Scientific machine learning through physics-informed neural networks: where we are and what's next, 2022, arXiv preprint arXiv:2201.05624.
[17] Kurt Hornik, Maxwell Stinchcombe, Halbert White, Multilayer feedforward networks are universal approximators, Neural Netw. 2 (5) (1989) 359–366.
[18] Isaac E. Lagaris, Aristidis Likas, Dimitrios I. Fotiadis, Artificial neural networks for solving ordinary and partial differential equations, IEEE Trans. Neural Netw. 9 (5) (1998) 987–1000.
[19] Isaac E. Lagaris, Aristidis C. Likas, Dimitris G. Papageorgiou, Neural-network methods for boundary value problems with irregular boundaries, IEEE Trans. Neural Netw. 11 (5) (2000) 1041–1049.
[20] Maziar Raissi, George Em Karniadakis, Hidden physics models: Machine learning of nonlinear partial differential equations, J. Comput. Phys. 357 (2018) 125–141.

[21] Zhiping Mao, Ameya D. Jagtap, George Em Karniadakis, Physics-informed neural networks for high-speed flows, Comput. Methods Appl. Mech. Engrg. 360 (2020) 112789.
[22] Mehryar Mohri, Afshin Rostamizadeh, Ameet Talwalkar, Foundations of Machine Learning, MIT Press, 2018.
[23] Ian Goodfellow, Yoshua Bengio, Aaron Courville, Deep Learning, MIT Press, 2016.
[24] Yann LeCun, Yoshua Bengio, Geoffrey Hinton, Deep learning, Nature 521 (7553) (2015) 436–444.
[25] Russel E. Caflisch, Monte carlo and quasi-monte carlo methods, Acta Numer. 7 (1998) 1–49.
[26] Atilim Gunes Baydin, Barak A. Pearlmutter, Alexey Andreyevich Radul, Jeffrey Mark Siskind, Automatic differentiation in machine learning: a survey, J. Marchine Learn. Res. 18 (2018) 1–43.
[27] Stefano Markidis, The old and the new: Can physics-informed deep-learning replace traditional linear solvers? Front. Big Data (2021) 92.
[28] Andrés Beltrán-Pulido, Ilias Bilionis, Dionysios Aliprantis, Physics-informed neural networks for solving parametric magnetostatic problems, IEEE Trans. Energy Convers. (2022).
[29] Subin Shrestha, Kevin Chou, A study of transient and steady-state regions from single-track deposition in laser powder bed fusion, J. Manuf. Process. 61 (2021) 226–235.
[30] Erik R. Denlinger, Vijay Jagdale, G.V. Srinivasan, Tahany El-Wardany, Pan Michaleris, Thermal modeling of Inconel 718 processed with powder bed fusion and experimental validation using in situ measurements, Addit. Manuf. 11 (2016) 7–15.
[31] Daniel Moser, Michael Cullinan, Jayathi Murthy, Multi-scale computational modeling of residual stress in selective laser melting with uncertainty quantification, Addit. Manuf. 29 (2019) 100770.
[32] Zhibo Luo, Yaoyao Zhao, Efficient thermal finite element modeling of selective laser melting of Inconel 718, Comput. Mech. 65 (3) (2020) 763–787.
[33] Erik R. Denlinger, Michael Gouge, Jeff Irwin, Pan Michaleris, Thermomechanical model development and in situ experimental validation of the Laser Powder-Bed Fusion process, Addit. Manuf. 16 (2017) 73–80.
[34] Ning An, Guangyu Yang, Kun Yang, Jian Wang, Meie Li, Jinxiong Zhou, Implementation of Abaqus user subroutines and plugin for thermal analysis of powder-bed electron-beam-melting additive manufacturing process, Mater. Today Commun. 27 (2021) 102307.
[35] John Goldak, Aditya Chakravarti, Malcolm Bibby, A new finite element model for welding heat sources, Metall. Trans. B 15 (2) (1984) 299–305.
[36] Zhengtao Gan, Yanping Lian, Stephen E. Lin, Kevontrez K. Jones, Wing Kam Liu, Gregory J. Wagner, Benchmark study of thermal behavior, surface topography, and dendritic microstructure in selective laser melting of Inconel 625, Integr. Mater. Manuf. Innov. 8 (2) (2019) 178–193.
[37] John Goldak, M. Bibby, J. Moore, R. House, B. Patel, Computer modeling of heat flow in welds, Metall. Trans. B 17 (3) (1986) 587–600.
[38] Zhidong Zhang, Yuze Huang, Adhitan Rani Kasinathan, Shahriar Imani Shahabad, Usman Ali, Yahya Mahmoodkhani, Ehsan Toyserkani, 3-Dimensional heat transfer modeling for laser powder-bed fusion additive manufacturing with volumetric heat sources based on varied thermal conductivity and absorptivity, Opt. Laser Technol. 109 (2019) 297–312.
[39] Andrew J. Pinkerton, Lin Li, Modelling the geometry of a moving laser melt pool and deposition track via energy and mass balances, J. Phys. D: Appl. Phys. 37 (14) (2004) 1885.
[40] Fabricio Castro, Artificial neural network architecture generator, 2022, MATLAB Central File Exchange.
[41] Dong C. Liu, Jorge Nocedal, On the limited memory BFGS method for large scale optimization, Math. Program. 45 (1) (1989) 503–528.
[42] Jan Morez, Jan Sijbers, Floris Vanhevel, Ben Jeurissen, Constrained spherical deconvolution of nonspherically sampled diffusion MRI data, Hum. Brain Mapp. 42 (2) (2021) 521–538.
[43] Pooriya Gh Ghanbari, Rafal Wrobel, Bastian Rheingans, Thomas Mayer, Leinenbach Christian, Edoardo Mazza, Ehsan Hosseini, 3D finite element thermal analysis of laser powder-bed fusion: Adaptive-local/global multiscale approach and experimental validation, 2023 submitted for publication.
[44] Michael D. McKay, Richard J. Beckman, William J. Conover, A comparison of three methods for selecting values of input variables in the analysis of output from a computer code, Technometrics 42 (1) (2000) 55–61.